carbonaceous chondrites, to be $^{12}C/^{13}C \simeq 92$, whereas the isotopic ratio for the Cβ structure, containing Xe in s-processed ratio (as produced in AGB stars themselves), has been measured[25] to be $^{12}C/^{13}C \simeq 42$.

An identification of Cβ structures as SiC grains in the Murray meteorite has now been announced[26,27] and the details in the announced analysis are in full agreement with the theory presented above for the formation of Cδ and Cβ inclusions in carbonaceous chondrites. Enlightening discussions with H. Nørgård and E. H. Olsen are greatly acknowledged. This work has been supported by the Danish Natural Science Research Council.

Received 3 December 1987; accepted 27 January 1988.

1. Lewis, R. S., Ming, T., Wacker, J. F., Anders, E. & Steel, E. *Nature* **326**, 160-162 (1987).
2. Roy, R. *Nature* **325**, 17-18 (1987).
3. Clayton, D. D. *Astrophys. J.* **199**, 765-769 (1975).
4. Schmid-Burgk, J. & Scholz, M. in *Physical Processes in Red Giants* (eds Iben, I, Jr. & Renzini, A.) 341-346 (Reidel, Dordrecht, 1981).
5. Draine, B. T. in *Physical Processes in Red Giants* (eds Iben, I, Jr. & Renzini, A.) 317-333 (Reidel, Dordrecht, 1981).
6. Salpeter, E. E. *Rev. Mod. Phys.* **46**, 433-436 (1974).
7. Eriksson, K., Gustafsson, B., Jørgensen, U. G. & Nordlund, Å. *Astr. Astrophys.* **132**, 37-44 (1984).
8. Jørgensen, U. G., Almlöf, J. & Siegbahn, P. E. M. *J. Chem. Phys.* (submitted).
9. Jørgensen, U. G. *Thesis*, Copenhagen Univ., 1987.
10. Renzini, A. & Voli M. *Astr. Astrophys.* **94**, 175-193 (1981).
11. Bertelli, G., Bressan, A. G. & Chiosi, C. *Astr. Astrophys.* **150**, 33-52 (1985).
12. Woosley, S. E. in *Nucleosynthesis and Chemical Evolution* (eds Hauck, B., Maeder, A. & Meynet, G.) 1-195 (Geneva Observatory, 1986).
13. Clayton, D. D. *Proc. Lunar Planet. Sci.* **12B**, 1781-1802 (Pergamon Press, Oxford, 1981).
14. Lambert, D. L. in *Cool Stars with Excesses of Heavy Elements* (eds Jaschek, M. & Keenan, P. C.) 191-223 (Reidel, Dordrecht, 1985).
15. Lewis, R. S. & Anders, E. *Astrophys. J.* **247**, 1122-1124 (1981).
16. Miller, G. E. & Scalo, J. M. *Astrophys. J.* **263**, 259-268 (1982).
17. Strömgren, B. in *The Galaxy* (eds Gilmore, G. & Carswell, R.) (Reidel, Dordrecht, in the press).
18. Olsen, E. H. *Ast. Astrophys. Suppl.* **57**, 443-466 (1984).
19. Peimbert, M. & Torres-Peimbert, S. *Astrophys. J.* **193**, 327-333 (1974).
20. Richer, H. B. & Westerlund, B. E. *Astrophys. J.* **264**, 114-125 (1983).
21. Cook, K. H., Aaronson, M. & Norris, J. *Astrophys. J.* **305**, 634-644 (1986).
22. Reimers, D. *Mem. Soc. Roy. Sci. Liege. Ser. 6* **8**, 369-382 (1975).
23. Iben, I. Jr & Renzini, A. *Ah. Rev. Astr. Astrophys.* **21**, 271-342 (1983).
24. Lambert, D. L., Gustafsson, B., Eriksson, K. & Hinkle, K. H. *Astrophys. J. Suppl.* **62**, 373-425 (1986).
25. Lewis, R. S. & Anders, E. *Scient. Am.* **249**, 54-66 (1983).
26. Bernatowicz, T. *et al. Nature* **330**, 728-730 (1987).
27. Zinner, E., Ming, T. & Anders, E. *Nature* **330**, 730-732 (1987).

Gas and dust jets in the inner coma of comet Halley

Cristiano B. Cosmovici*, Gottfried Schwarz†, Wing-Huen Ip‡ & Peter Mack§

* Istituto di Fisica dello Spazio Interplanetario, CNR, 00044 Frascati, Italy
† DFVLR, Hauptabteilung Angewandte Datentechnik, 8031 Oberpfaffenhofen, FRG
‡ Max-Planck-Institut für Aeronomie, 3411 Katlenburg-Lindau, FRG
§ South African Astronomical Observatory, P.O. Box 9, Observatory 7935, South Africa

Cyanogen (CN) jets were discovered in comet Halley by applying an image processing ring masking technique to ground-based observations[1,2]. We now report the detection of dust, C_2, C_3, CN and ([O I]+NH_2) jet features in comet Halley during the period of the spacecraft Giotto encounter (13–18 March 1986). With absolute flux measurements, careful continuum subtraction and an improved ring-masking technique, we have achieved an unambiguous separation of the gas and dust components of the cometary coma emissions. A comparison of the morphologies of these gas and dust jets provides important information about the anisotropic dynamical processes in the cometary coma and on the surface of comet Halley's nucleus.

The observations were carried out between 13-18 March 1986, around the time of the Giotto flyby of comet Halley on 13 March. The aim was to compare ground-based observations with close-up images taken by the Giotto camera[3-5]. We used the charge-coupled device (CCD) camera system of the 1.9-m telescope at the South African Astronomical Observatory (SAAO), Sutherland, South Africa. Preliminary results, obtained with 23 different filters (including the filter set for the Halley Multicolour Camera of Giotto), have been reported[3-6]. Further information about the instrumental and observational data and about the filters used is given in Tables 1 and 2. Table 3 summarizes the image data for the observations.

Table 1 Instrumental and observational data

Observing site	Sutherland (SAAO)
Telescope	1.9-m Cassegrain $f/6.5$ reduced
Detector	Thinned RCA 53612 CCD 360×512 pixels
Imaging area	318×510 pixels corresponding to: 2.97×4.76 arc min^2 Average at comet: $(120 \times 10^3 \times 190 \times 10^3)$ km^2
Image resolution	0.56 arc s per pixel $\approx$370 km

Table 2 Filters used with the CCD camera system

Filters	Wavelength (Å)	FWHM* (Å)
International Halley Watch		
Continuum blue (BC)	3,650	80
CN	3,871	50
C_3	4,060	70
CO^+	4,260	70
Mid continuum (MC)	4,845	65
C_2	5,139	90
Max-Planck Institute		
H_2O^+	6,193	43
H_2O^+ continuum	6,253.5	18.7
[O I]+NH_2	6,297	9.5
([O I]+NH_2) continuum	6,248	8

* FWHM denotes full width at half maximum.

The technique for absolute photometric calibration as suggested by the International Halley Watch (IHW) for near-nucleus studies was used. As reported[3], a locally adaptive ring-masking technique was used to enhance the jet features and it was shown that gas and dust jets can be resolved at different wavelengths in the cometary coma of comet Halley. The images obtained with narrow-band filters contain both gas emissions and continuum which stems from sunlight scattered on solid particles. After absolute calibration of all filters an accurate continuum subtraction was carried out by precisely co-aligning (that is superimposing with correct positioning) the gas and continuum filter images. In most cases, image edges had to be cut to remove non-overlapping areas and to eliminate blemishes caused by stars. For these reasons, the full images covering $120{,}000 \times 190{,}000$ km^2 could not be used for ring masking and the analysis was restricted to an area with a diameter of 70,000 km around the nucleus. Finally, the jet structures in the continuum subtracted images were enhanced by ring masking[3].

In the case of H_2O^+ and ([O I]+NH_2) emission we could use special narrow band filters with the continuum emission located very close to the gas emission wavelength (Table 2). Therefore, the background subtraction is quite accurate. In the case of the IHW filters the continuum wavelengths (3,650 and 4,845 Å) lie far from the C_3 and CO^+ emissions, but as we had no jet structures in the continuum blue (3,650 Å) and the CO^+ (4,260 Å) images showed only dust jet structures, we used these filters as continuum subtraction for CN (3,871 Å) and C_3 (4,060 Å), taking into account that the solar flux does not change appreciably in this wavelength region (Fig. 2, ref. 3). The 4,845 Å continuum filter was only used for subtraction from C_2 (5,139 Å). In the following, we concentrate on the images taken

Table 3 Image data for observations during Giotto encounter

Filter	Date (March 1986)	Exposure time (s)
B.C.	14.099	30
CN	14.108	30
C_3	14.101	30
CO^+	14.104	30
M.C.	14.103	30
C_2	14.105	30
H_2O^+	14.144	300
H_2O^+ continuum	14.150	250
B.C.	15.092	60
CN	15.101	60
C_3	15.094	60
CO^+	15.099	60
M.C.	15.096	60
C_2	15.100	30
H_2O^+	15.106	60
H_2O^+ continuum	15.114	60
B.C.	17.048	120
CN	17.059	60
C_3	17.051	60
CO^+	17.055	60
M.C.	17.053	60
C_2	17.057	60
[O I] + NH_2	17.153	300
([O I] + NH_2) continuum	17.163	300
B.C.	18.058	60
CN	18.074	60
C_3	18.059	60
CO^+	18.069	60
M.C.	18.067	60
C_2	18.071	60
O I + NH_2	18.087	180
([O I] + NH_2) continuum	18.095	180

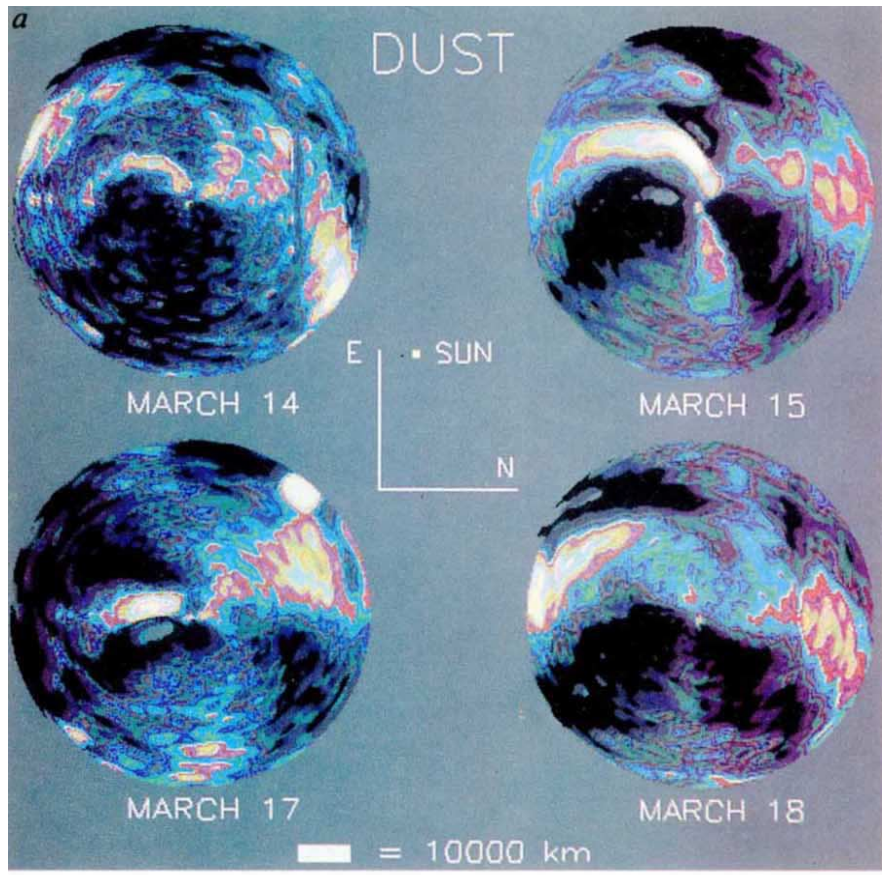

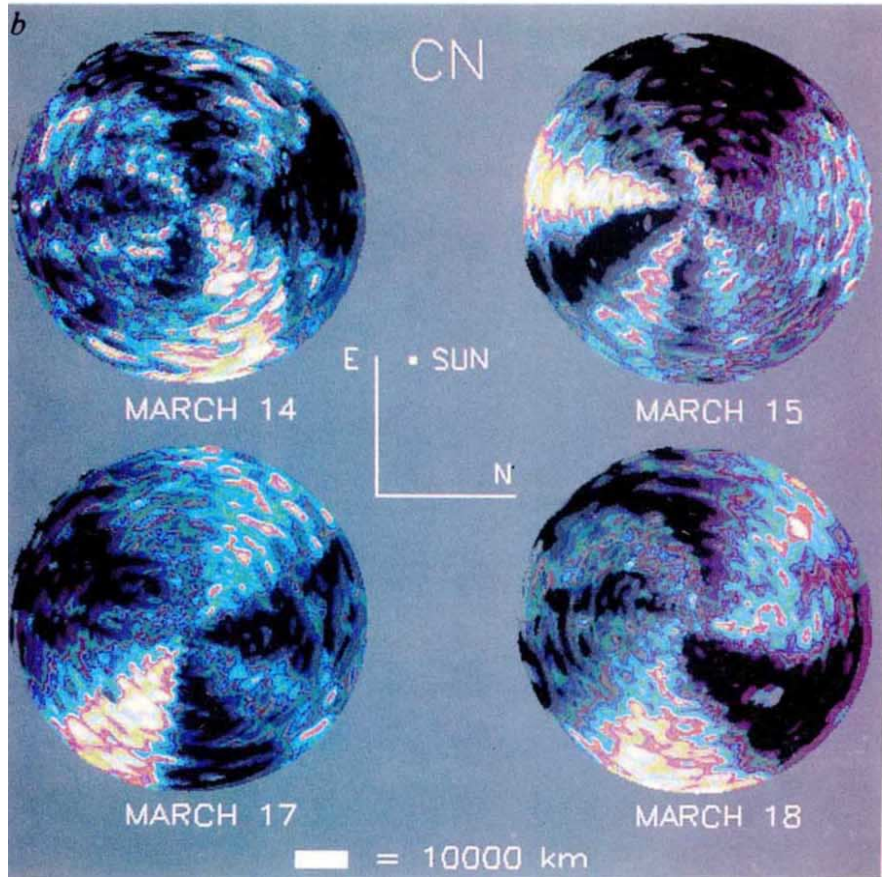

Fig. 1 *a*, Dust jets enhanced by ring masking in a region of 70,000 km around the nucleus; *b*, CN jets; *c*, C_2 jets; *d*, C_3 jets; *e*, [O I] + NH_2 jets.

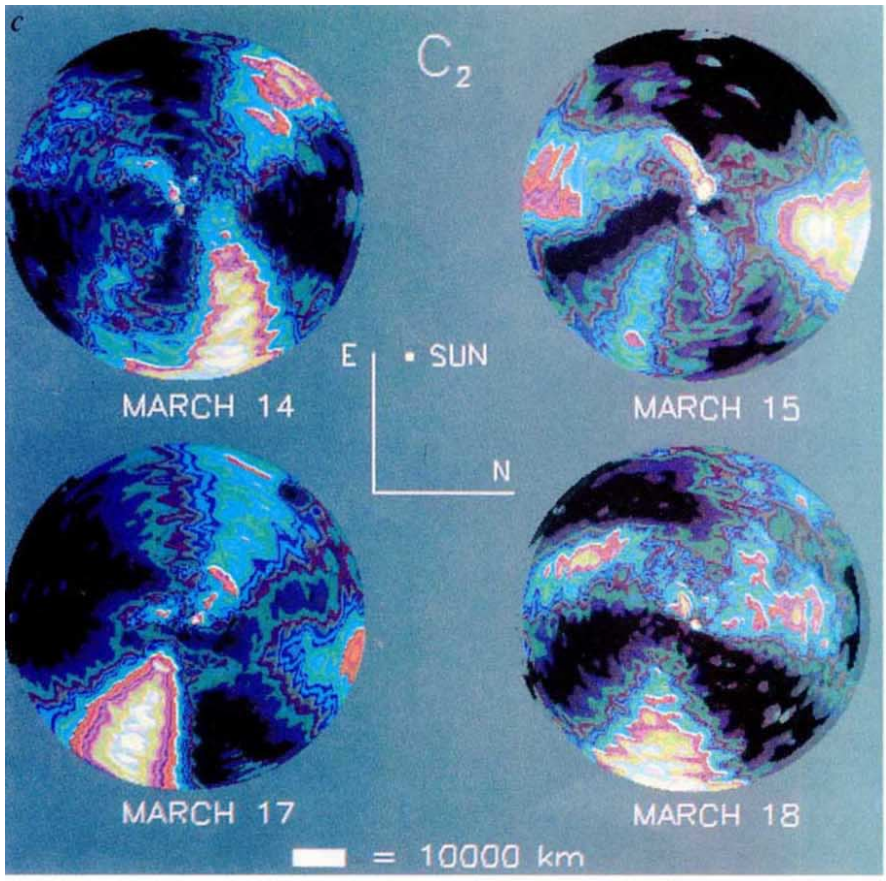
c
C2
E
SUN
N
MARCH 14
MARCH 15
MARCH 17
MARCH 18
= 10000 km

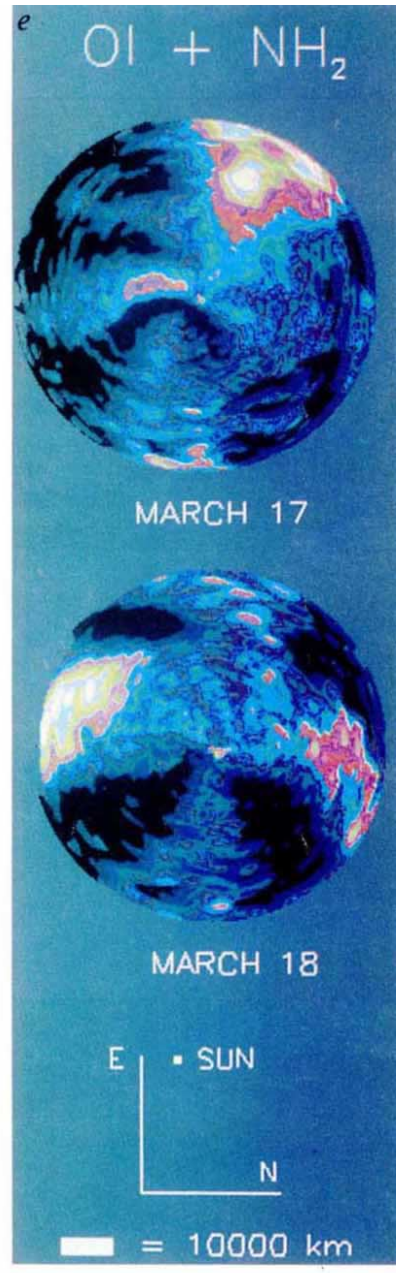
e
OI + NH2
MARCH 17
MARCH 18
E
SUN
N
= 10000 km

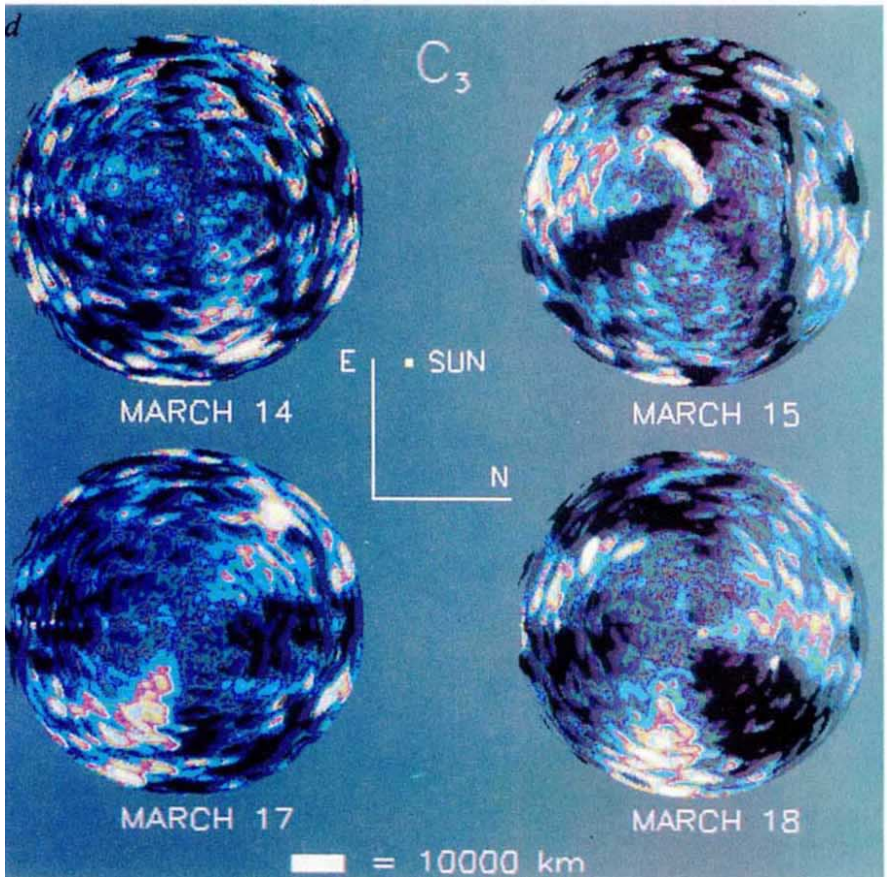
d
C3
E
SUN
N
MARCH 14
MARCH 15
MARCH 17
MARCH 18
= 10000 km

on 14, 15, 17 and 18 March using the IHW filter set and the special set of narrow-band filters for the H_2O^+ ions and the ([O I]+NH_2) emission, as detailed in Tables 2 and 3. The jet enhanced images obtained for dust, CN, C_2, C_3 and ([O I]+NH_2) are shown in Fig. 1.

Dust. Dust jets have been observed extensively from the Giotto and Vega and from the ground[3-10]. Their formation is presumably caused by emissions of gas and dust in discrete regions on the surface of the cometary nucleus. The morphology and the time variation of these dust jet features have been used to deduce the rotation period(s) of comet Halley[10-12]. Our measurements covering five nights in March 1986 are not sufficient to derive rotational periods but could be correlated with other ground-based observations, for example, with observations taken from Chile and Australia (having a time shift of 8 hours) and with space observations. Figure 1*a* shows the dust morphology during four nights using the continuum filter at 4,845 Å. The continuum at 6,253 Å shows the same features. Note that, as a rule, no jets are seen in the continuum at 3,650 Å.

On 15 March a strong outburst caused an increase of the peak total luminosity in the red filter image by a factor of four with respect to the 14 March observation[4-5]. This outburst can clearly be seen as the long bright spiral jet to the south-east with a length of ~40,000 km. On all images there are jet structures moving away from the nucleus in agreement with the view that these dust jets are generated at different time intervals. Dust jets are only observable in the red wavelength region because the sunlight is mainly scattered by grains with diameters $d > \lambda >$ 4,000 Å, that is, the Mie and not the Rayleigh scattering is responsible for the visibility of the dust jets.

CN, C_2, C_3. A'Hearn *et al.*[2] already observed that the shape of the CN and C_2 jets is different from the continuum jets at 4,845 Å, but their measurements were still affected by the continuum band which is very strong in the case of the C_2 jets. From our measurements, obtained during a different period but with accurate continuum subtraction, we observe the following. First, CN, C_2 and C_3 emissions consist of jet structures different from the dust continuum; second, C_2 jets are very bright and well defined with general structures mostly similar to their CN counterparts; third, on 15 March, during the outburst, there appeared a strong conical CN jet to the south which was not observed with any other filter. We therefore conclude that C_2 and C_3 were formed in the same regions as CN in the gas jets on 14, 17 and 18 March. On 15 March a particular event led to the formation of CN only in a region south of the nucleus with an extent of more than 50,000 km. Several mechanisms have been proposed to explain the formation of CN jets. These include sublimation from the sub-micrometre organic CHON grains[1,13] and emissions from the cometary nucleus surface with chemical inhomogeneities[14]. The DIDSY instrument on Giotto provided information on the cumulative flux distributions of the dust particles in the coma of comet Halley[15,16]. The data were used to estimate that the total mass production rate of the sub-micrometre grains is approximately 10^3 g s^{-1}. This value is too low to account for the C_2 and CN jet production even if the radical jets contain no more than 10% of the total C_2 and CN emissions (for a relative abundance of 10^{-3}-10^{-2} for C_2 and CN, the corresponding mass production rate is about 2×10^4-2×10^5 g s^{-1}). This estimate thus casts doubt on the validity of the CHON grain origin (see also refs 2, 14).

The alternative idea of direct emission from the surface of the nucleus[14] requires that the radiation-pressure acceleration should be similar for both C_2 and CN. If not, we expect a separation of the two components at large distances from the cometary nucleus (the same argument applies if we assume sub-micrometre grains as the parent particles of the C_2 and CN radicals as these small dust particles will be sorted out from the larger particles by the solar radiation pressure). In view of these issues, both proposals should be studied in more detail. One additional effect which also deserves consideration has to do with the ion chemistry such as $H_2O^+ + HCN \rightarrow H_2CN^+ + OH$, followed by an electron dissociative recombination process $H_2CN^+ + e \rightarrow CN + H_2$. In this way, the presence of plasma structures (that is, ion streamers or envelopes) in the cometary ionosphere could also lead to the generation of jet-like features in CN and C_2. Because of the lack of ion emission profiles, it is not possible to test this hypothesis at present. Furthermore, any increase of the CN and C_2 radicals in the tailward side due to the ion chemical processes in the plasma tail, would superimpose on the asymmetry caused by the solar radiation pressure acceleration. Because H_2CN^+ ions could be quite abundant in the inner ionosphere[17], it is important that this possibility is not overlooked.

[O I]+NH_2. One new feature in our CCD observations is the presence of anisotropic patterns in the brightness of the forbidden [O I] emission at 6,300 Å. Our filter bandwidth permits the detection of the NH_2 (0, 8, 0 → 0, 0, 0) band at 6,294.45, 6,295.83, 6,297.32, 6,298.62 Å. In the case of the global anisotropy, because of the short lifetimes of NH_3 and NH_2 molecules due to photodissociation, most of the NH_2 emission can be shown to be limited to a distance of $\sim2\times10^4$ km from the nucleus. The contribution from NH_2 is therefore small beyond this region. As for the jets, whose brightness increment is typically just a few per cent of the general background, one cannot rule out the possibility that [O I] and NH_2 might be released from small dust streamers—even though this would imply different source particles for the [O I]+NH_2 jets as well as the CN and C_2 jets. Because the ring-masking technique subtracts atmospheric oxygen automatically from our measurements, we can assume that the ([O I]+NH_2)/dust ratio in a region of ~70,000 km around the nucleus is ~8. We obtain [O I]/dust = 5.3, NH_2/dust = 2.7. In the following, we shall assume that most of the asymmetry and jet features seen in Fig. 1*e* are due to the [O I] atoms. We consider that the [O I] images are of great interest as they carry unique information on the distribution of the H_2O molecules in the coma. So far, except for a brief mention of the asymmetry in the OH brightness distribution as observed by IUE[18] and the inference from the near-infrared spectrometer experiment on Vega of a sunward jet of the H_2O vapour[19], no report has yet been published describing the global distribution of the water molecules.

Of the two photolytic processes[20,21], $H_2O + h\nu \rightarrow H_2 + O^1D$ and $OH + h\nu \rightarrow H + O^1D$, the first is more important in the region covered by our observations ($r < 10^5$ km). Thus, the [O I] observations on 17 and 18 March can be used to make the following deductions. First, the water production rate and hence the surface sublimation process are not as isotropic as might have been inferred from the neutral mass spectrometer observations at comet Halley[22,23]. According to our present analysis, the degree of anisotropy is quite significant, that is, an amplitude of $\Delta I/\langle I\rangle \approx 30\%$ at a radial distance of $r = 5{,}000$ km on 17 March and $\Delta I/\langle I\rangle \approx 19\%$ on 18 March. This variation probably reflects the presence of temporal variations in the outgassing process from the nucleus. Second, the [O I] jets show a similar morphology to those of the dust particles only on 18 March, but the south-pointing jet is ~6,000 km broader. They are also separated from the CN and C_2 jets. On 17 March, in addition to a wide jet pointing to the left which is related to a similar dust feature, the [O I] emission has a strong increase in the sunward-pointing direction.

One aim of the imaging observations using the pair of filters with central wavelengths at 6,193 Å and 6,253 Å is to resolve the emission from the H_2O^+ ions in the coma. The bandwidth of the filters was very narrow in comparison with the IHW filters (see Table 2). Because of the very strong emission from the dust continuum within a radial distance of a few 10^4 km, however a determination of the morphologies of the ion emission is not yet feasible.

In summary, detailed image processing of the ground-based observations from South Africa taken during the Giotto encoun-

ter has revealed a wealth of information on the global and local structures of the gas and dust comae of comet Halley. While our results confirm and expand on the discovery of CN jets by A'Hearn *et al.*[1,2], the unambiguous detection of C_2, C_3 and ($[O\ I]+NH_2$) jets separated from dust permit a more direct comparison with theoretical models concerning the formation of radicals and complex molecules on sub-micrometre grains. Moreover, the timing of our SAAO observations allows some quantitative comparisons of the production rate of the C_2 and CN radicals and of the dust grains. Our analysis suggests that the model of evaporation from the CHON particles may be limited by the estimated mass ejection rate of the sub-micrometre grains ($<10^3$ g s^{-1}), a potential difficulty noted previously[2]. The mechanism of direct ejection of CN and C_2 radicals from the surface of the nucleus[14], on the other hand, has to be evaluated according to the temporal variations of the jet features under the influence of solar radiation pressure and nucleus rotation. Clarification must await detailed model study. The presence of a strong anisotropy in the [O I] distribution, directly related to the outgassing pattern of the water vapour, is quite clear in our filtered image specially designed for imaging [O I] emission. A comparison of the observed asymmetry with theoretical models[24-27] will be essential in the understanding of the surface sublimation of comet Halley at the time of the Giotto encounter.

We thank all SAAO staff, and Dr K. Schmidt, E. Krieg and E. Mikusch of DFVLR. We also thank Mr H. Lauche at MPAe for providing the [O I] filter set and technical advice. The campaign in South Africa was financed by the Observatory of Padova on behalf of CNR.

Received 16 November 1987; accepted 22 January 1988.

1. A'Hearn, M. F. *et al. Nature* **324**, 649-651 (1986).
2. A'Hearn, M. F. *et al. Eur. Space Ag. spec. Publ.* **250**(1), 483-486 (1986).
3. Cosmovici, C. B., Mack, P., Schwarz, G., Craubner, A. & Ip, W. I. *Eur. Space Ag. spec. Publ.* **278**, 195-207 (1987).
4. Cosmovici, C. B., Mack, P., Craubner, H. & Schwarz, G. *Eur. Space Ag. spec. Publ.* **250**(2), 151-155 (1986).
5. Cosmovici, C. B. *et al. Eur. Space Ag. spec. Publ.* **250**(2), 375-379 (1986).
6. Ip, W.-H., Cosmovici, C. B., Mack, P., Craubner, A. & Schwarz, G. *Eur. Space Ag. spec. Publ.* **278**, 271-275, (1987).
7. Grün, E. *et al. Nature* **321**, 144-147 (1987).
8. Sagdeev, R. Z. *et al. Nature* **321**, 262-266 (1986).
9. Keller, H. U. *et al. Nature* **321**, 320-326 (1986).
10. Sekanina, Z. & Larson, S. M. *Nature* **321**, 357-361 (1986).
11. Wilhelm, K. *Nature* **327**, 27-31 (1987).
12. Sekanina, Z *Adv. Space Res.* **5**, 307-316 (1986).
13. Kissel, J. *et al. Nature* **321**, 336-337 (1986).
14. Combi, M. R. *Icarus* **71**, 178-191 (1987).
15. McDonnell, J. A. M. *et al. Nature* **321**, 338-341 (1986).
16. McDonnell, J. A. M. *et al. Eur. Space Ag. spec. Publ.* **250**(2), 25-38 (1986).
17. Ip, W.-H. *Adv. Space Res.* **5**, 233-245 (1986).
18. Festou, M. C. *et al. Nature* **321**, 361-363 (1986).
19. Krasnopolsky, V. A. *et al. Eur. Space Ag. spec. Publ.* **250**(1), 459-464 (1986).
20. Roesler, F. L. *et al. Eur. Space Ag. spec. Publ.* **250**(1), 413-415 (1986).
21. Spinrad, H., McCarthy, P. J. & Strauss, M. A. *Eur. Space Ag. spec. Publ.* **250**(1), 437-438 (1986).
22. Krankowsky, D. *et al. Nature* **321**, 326-329 (1986).
23. Gringauz, K. I. *et al. Nature* **321**, 282-285 (1986).
24. Kitamura, Y. *Icarus* **66**, 241-257 (1986).
25. Kömle, N. & Ip, W.-H. *Eur. Space Ag. spec. Publ.* **250**(1), 523-527 (1986).
26. Kömle, N. & Ip, W.-H. *Eur. Space Ag. spec. Publ.* **278**, 247-254 (1987).
27. Kitamura, Y. *Icarus* (in the press).

Comparison of SAGE II solar extinction data with airborne measurements of atmospheric backscattering in the troposphere and lower stratosphere

J. M. Vaughan*, D. W. Brown*, P. H. Davies*, C. Nash*, G. Kent† & M. P. McCormick‡

* Royal Signals and Radar Establishment, St Andrews Road, Great Malvern, Worcestershire WR14 3PS, UK
† Science and Technology Corporation, 101 Research Drive, Hampton, Virginia 23666, USA
‡ NASA Langley Research Center, Hampton, Virginia 23665, USA

Since October 1984 the SAGE II limb sounding satellite has been measuring the extinction $\sigma(\lambda)$ of the Earth's atmosphere in seven wavebands. The extinction at the longest wavelength, σ (1.02 μm), is largely due to particulate material (aerosols) in the atmosphere. It is of considerable interest to relate these extinction values to the strength of atmospheric backscattering at this and longer wavelengths. In particular, atmospheric backscattering coefficients $\beta(\pi, \lambda)$ in the 9–11 μm range are important because projected performance of a satellite-borne CO_2 lidar for global wind measurement depends critically on their magnitude (the π signifiies backscatter). In April 1986, during passage of the SAGE II satellite, the first simultaneous measurements of β (π, 10.6 μm) were made with an airborne CO_2 lidar. Individual ratios of β (π, 10.6 μm) and SAGE II extinction σ (1.02 μm) are in reasonable accord with previously calculated values, but the trend with height shows a distinctly nonlinear relation , which is probably attributable to a steadily changing size distribution of aerosols.

The NASA Stratospheric Aerosol and Gas Experiment (SAGE II)[1] on the Earth Radiation Budget Satellite (ERBS) is in a 610 km altitude circular orbit with a 57° inclination yielding global coverage ranging between 80° S and 80° N latitude every few weeks. Extinction measurements of solar radiation are made twice in each orbit during spacecraft sunrise and sunset (units of extinction, m^{-1}). The satellite orbital period is ~100 min so there are approximately 30 sampling opportunities per day.

Table 1 Comparison of local-atmospheric-backscatter coefficient (from the aircraft) and long-path extinction (from the satellite)

Altitude (km)	β (π, 10.6 μm) (10^{-10} m^{-1} sr^{-1})	σ (1.02 μm) (10^{-7} m^{-1})	$\frac{\beta\ (\pi, 10.6\ \mu m)}{\sigma(1.02\ \mu m)}$ (10^{-4} sr^{-1})
6.5*	530.8	36.93	14.37
7.5	11.83	19.15	6.18
8.5	4.558	13.54	3.37
9.5†	2.198	11.39	1.93
10.5*	1.551	9.318	1.66
11.5*	1.132	8.563	1.32
12.5*	1.066	8.503	1.25

Data recorded at sunset on 21 April 1986. The β (π, 10.6 μm) values are averages over 1 km height intervals for comparison with the satellite extinction values of σ (1.02 μm) which are deconvolved with a spatial-height resolution of 1 km.
* Cloud-contaminated value.
† Values in the stratosphere.

During a sunrise or sunset event, measurements of solar radiation are taken from a tangent height of 150 km (where there is no atmospheric attenuation) to the Earth's surface (or until the Sun is obscured by clouds). The solar radiance data are mathematically inverted into values of atmospheric extinction versus tangent altitude (at 1 km height intervals) and with approximately 1 km vertical resolution; the corresponding horizontal viewing paths are approximately 250 km long. These total extinction profiles are then separated into aerosol-extinction and gaseous-constituent-concentration profiles.

On three successive days, 19–21 April 1986, SAGE II measurements were made at sunset near the United Kingdom. The RSRE True Airspeed (LATAS) lidar was flown as close as possible to the atmospheric paths observed by the satellite. The LATAS equipment was installed aboard an HS 125 aircraft (maximum ceiling 13 km above sea level) operated from the Royal Aircraft Establishment (Bedford). The lidar, which incorporates a continuous-wave CO_2 laser at 10.6 μm of ~4 W output, has been operated for over five years with good reliability; extensive measurements of true airspeed, windshear, microbursts, turbulence and pressure error have been made and reported with a description of the complete equipment[2]. The continuous-wave